ANNUAL REVIEWS

Annual Review of Materials Research

Cation Dynamics in Hybrid Halide Perovskites

Eve M. Mozur and James R. Neilson

Department of Chemistry, Colorado State University, Fort Collins, Colorado 80523, USA; email: jrn@colostate.edu

Annu. Rev. Mater. Res. 2021. 51:269–91

First published as a Review in Advance on May 24, 2021

The *Annual Review of Materials Research* is online at matsci.annualreviews.org

https://doi.org/10.1146/annurev-matsci-080819-012808

Keywords

hybrid perovskite, neutron scattering, semiconductor, spectroscopy

Abstract

Hybrid halide perovskite semiconductors exhibit complex, dynamical disorder while also harboring properties ideal for optoelectronic applications that include photovoltaics. However, these materials are structurally and compositionally distinct from traditional compound semiconductors composed of tetrahedrally coordinated elements with an average valence electron count of silicon. The additional dynamic degrees of freedom of hybrid halide perovskites underlie many of their potentially transformative physical properties. Neutron scattering and spectroscopy studies of the atomic dynamics of these materials have yielded significant insights into their functional properties. Specifically, inelastic neutron scattering has been used to elucidate the phonon band structure, and quasi-elastic neutron scattering has revealed the nature of the uncorrelated dynamics pertaining to molecular reorientations. Understanding the dynamics of these complex semiconductors has elucidated the temperature-dependent phase stability and origins of defect-tolerant electronic transport from the highly polarizable dielectric response. Furthermore, the dynamic degrees of freedom of the hybrid perovskites provide additional opportunities for application engineering and innovation.

1. INTRODUCTION: HYBRID HALIDE PEROVSKITE SEMICONDUCTORS

Exciton: here, the coulombically attracted bound state of negative and positive charge carriers in a crystal

Polaron: the distortion of an ionic lattice in response to extra charges, akin to the Fröhlich mechanism

Phonon bottleneck: a bottleneck of heat-transporting phonons preventing electronic relaxation, such as the relaxation of "hot" carriers to the band edges

Rashba splitting: Broken inversion symmetry in the presence of strong spin-orbit coupling splits doubly degenerate bands into spin-up versus spin-down bands, limiting spin-allowed transitions

Hybrid halide perovskites and their structural derivatives have advantageous optoelectronic properties for a relatively wide range of applications. The tunable bandgap, defect tolerance, and long electronic excited-state lifetimes of these perovskites make them ideal semiconductors for photovoltaics (1, 2). The heavy elements in these materials also allow their use in X-ray and γ-ray detection (3, 4). Changing the composition or reducing the effective dimensionality changes the electronic structure and exciton binding energy to increase the efficiency of light emission; several materials even reemit white light intrinsically (5). This family of materials provides new opportunities for building the structure–property relationships of next-generation semiconductors.

Hybrid halide perovskites exhibit additional dynamic degrees of freedom in comparison to traditional compound semiconductors (e.g., CdTe, GaAs, TlBr). Materials such as $(CH_3NH_3)PbI_3$ and $(CH(NH_2)_2)PbI_3$ are plastic crystals, as schematically depicted in **Figure 1*a***: The organic cations exhibit translational symmetry with respect to their center of mass but without orientational order (7). The molecular sphere approximated by rotating the molecules can be used to compute a revised Goldschmidt tolerance factor based on the ionic radii of the constituent ions (8) (**Figure 1*b***), which is often employed to predict the formation of a crystal structure analogous to the mineral perovskite $CaTiO_3$ (9). Similar to oxide perovskites, halide perovskites typically undergo phase transitions on cooling, as characterized by a reduction in symmetry from cubic to tetragonal to orthorhombic that is related to cooperative tilting of the octahedral framework (10, 11). However, the rich and subtle details of these transitions and the resulting properties of each phase cannot be fully understood without considering the plastic crystalline nature of these materials (12).

Various advantageous electronic properties in hybrid perovskites have been attributed to their dynamic, plastic crystalline behavior. While long electronic excited-state lifetimes have been linked to collective dynamics of the extended octahedral framework (i.e., phonons) (13–17), such long-lived excited states are also linked to organic cation reorientational dynamics by way of giant polaron (18), phonon bottleneck (19, 20), or Rashba splitting–based (21) mechanisms

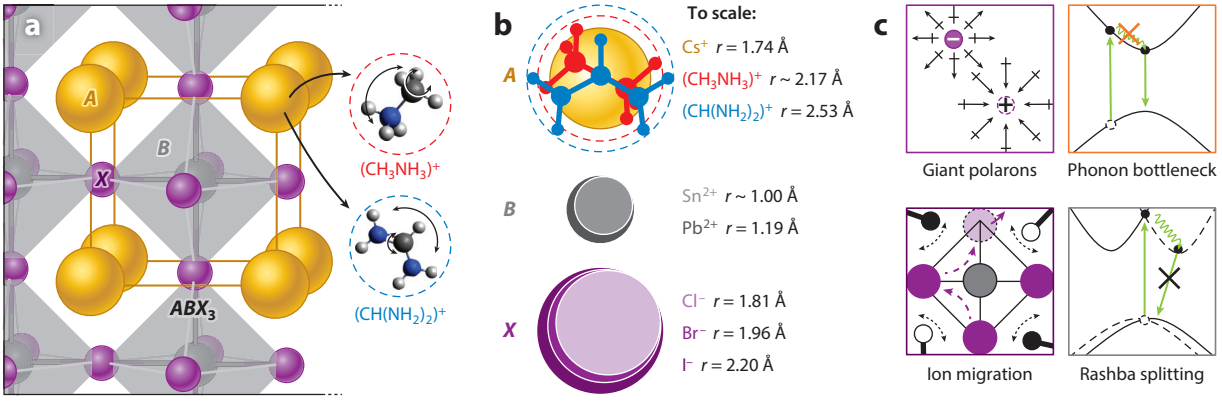

Figure 1

(*a*) Schematic illustration of the plastic crystalline nature of hybrid perovskites of the formula ABX_3, as well as the principal rotations of methylammonium, $(CH_3NH_3)^+$, and formamidinium, $(CH(NH_2)_2)^+$. (*b*) Diagram illustrating the scale of the various ions found in hybrid halide perovskites on the basis of their Shannon–Prewitt radii (6) or estimated molecular size (8). (*c*) Commonly proposed electron–phonon interactions in hybrid halide perovskites involving organic cation dynamics.

(described in more detail in Section 2.2.2) (**Figure 1*c***). Furthermore, the presence of an organic cation has been associated with the so-called self-healing of photoinduced defects (22) and aids in photoinduced ionic conductivity (23–25). The ionic mobility of hybrid halide perovskites is often linked to decomposition (26–29) and is hypothesized to relate to stationary atomic fluctuations (30), akin to the paddlewheel mechanism in materials studied for alkali ion conduction (31, 32). Similar dynamics are thought to influence relaxation pathways in layered perovskite derivatives of interest as phosphors (33, 34); the microscopic details remain an active area of research. Regardless of the proposed mechanism, the impressive defect-tolerant properties of hybrid halide perovskites advance high-efficiency photovoltaics (1, 35, 36). This review focuses on how neutron scattering (described in the sidebar titled Neutron Scattering: A Brief Primer), particularly quasi-elastic neutron scattering (QENS, described in the sidebar titled Quasi-Elastic Neutron Scattering: A Closer Look), has addressed questions related to these properties by characterizing the dynamic nature of organic cations in hybrid perovskite semiconductors.

Incoherent scattering: yields information independent of positional correlations

NEUTRON SCATTERING: A BRIEF PRIMER

Neutron scattering is a powerful tool to investigate the structure and dynamics of materials through analysis of the dynamic structure factor, $S(\boldsymbol{Q}, \omega)$ (**Figure 2*a***). The large large momentum of neutrons (relative to X-rays) allows them to couple strongly to atomic and molecular dynamics. The scattering cross section depends on interactions of the neutron with the nuclei within each atom and is therefore isotope dependent (37) (**Figure 2*b***) and provides complementary atomic contrast to X-ray scattering techniques that depend on the square of the atomic number. Therefore, short wavelengths (0.5–4 Å) are suitable for diffraction, while their energies (μeV–eV) are ideal for spectroscopy. The neutron scattering techniques most relevant for investigating the structure and dynamics of materials include neutron diffraction, quasi-elastic neutron scattering (QENS), and inelastic neutron scattering (INS), as summarized in **Figure 2**. INS probes the vibrational density of states between ∼5 and 1,000 meV. QENS probes dynamics on the μeV energy scale, encompassing molecular reorientations, translations, and diffusion. These dynamics map onto the dielectric response function illustrated in **Figure 2*e*,*f***.

QENS is complementary to other techniques sensitive to motions on 10^{-9}–10^{-12} s timescales, such as nuclear magnetic and optical spectroscopies [e.g., Brillouin light scattering (38) or ultrafast spectroscopy (39)].

QUASI-ELASTIC NEUTRON SCATTERING: A CLOSER LOOK

QENS is performed on neutron spectrometers with excellent energy resolution ($\Delta E \sim$ 1–3 μeV) and yields information about slow motions corresponding to relaxation of nearly stationary states, such as diffusion or molecular relaxation via translations or rotations. These relaxations provide a Doppler broadening of the elastic scattering as a result of the small energy transfer between neutrons and the moving nuclei in the sample.

To analyze the molecular motions, one can use a jump model, as molecules are assumed to reside in preferred orientations with jumps between well-defined orientations (40). The quasi-elastic line width relates to the timescale of this residence time between jumps (Lorentzian half-width at half-maximum $= \hbar/\tau$) (**Figure 2*a***). When analyzing purely incoherent scattering, the elastic incoherent structure factor (EISF), which equals $I_{\text{elastic}}/(I_{\text{elastic}} + I_{\text{quasi-elastic}})$, can be fitted with the jump model to extract the type of motion, including the local symmetry of motion, distance of motion, and geometry of the moving object, as illustrated in **Figure 2*c***.

Incoherent elastic scattering yields information about thermal motion, which follows a Q-dependent attenuation depending on the mean squared displacement (MSD) of atomic motion via the Debye–Waller factor, $\exp(-q^2\langle u^2\rangle/3)$, for isotropic, harmonic motion, as shown in **Figure 2*d***.

2. BACKGROUND: DYNAMICS AND ELECTRONIC PROPERTIES

The frontier electronic states of halide perovskites couple primarily to low-energy optical phonons. The influence of lattice dynamics on semiconductors typically revolves around a discussion of the scattering of charge carriers from electron–phonon coupling. In compound semiconductors with diamond-type structure, such as GaAs, optical phonons reside near ~40 meV; thus, they are not appreciably populated at room temperature and play a relatively small role in electron–phonon scattering processes (45). In contrast, halide perovskite optical phonons reside between ~5 and ~12 meV (**Figure 2**). Therefore, a complete understanding of the charge transport necessitates characterization of the electron–phonon coupling. In this section, we provide a brief overview of the importance of these collective dynamics in the context of light-absorbing hybrid semiconductors for photovoltaics, and then we discuss the presence and role of localized (i.e., aperiodic) dynamics and their proposed roles in influencing the optoelectronic performance of hybrid perovskites and related semiconductors.

2.1. Collective, Periodic Dynamics: Phonons

Optical phonons, derived primarily from the cooperative dynamics within the octahedral framework, drive the phase behavior of halide perovskites. Akin to the ferroelectric perovskite oxides

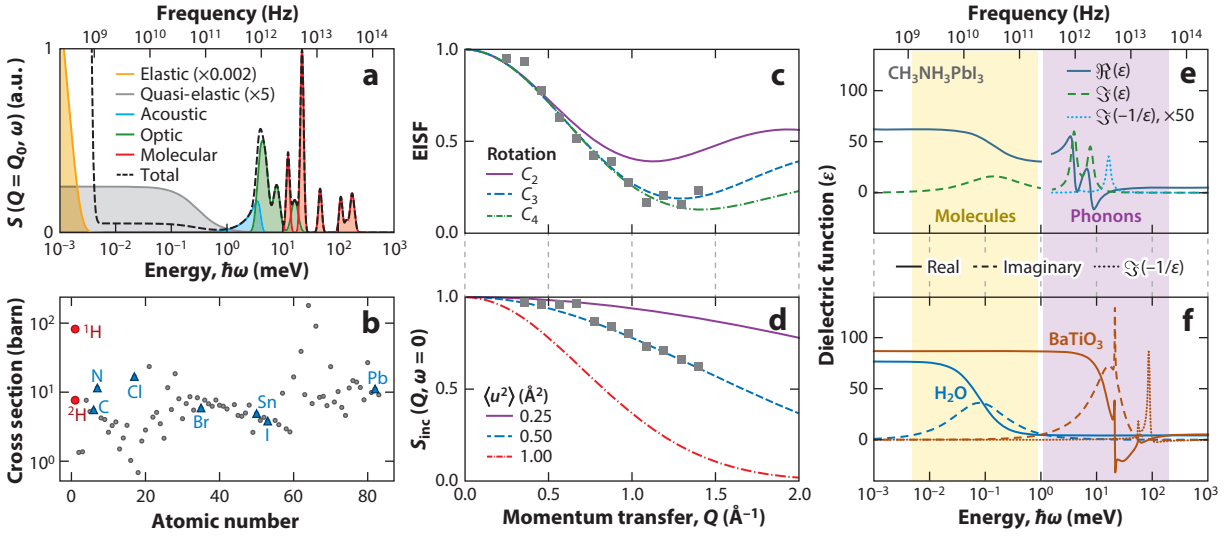

Figure 2

(*a*) Schematic representation of features observable in neutron spectroscopy, including elastic scattering from static atoms, quasi-elastic neutron scattering (QENS) from molecular reorientational dynamics, and inelastic neutron scattering from quantized lattice vibrations (acoustic and optical phonons) and molecular vibrations. (*b*) Neutron scattering cross section of different natural abundance–averaged elements (37), highlighting the large cross section of ^{1}H relative to the other elements germane to hybrid perovskites. (*c*) The elastic incoherent structure factor (EISF) used to extract details of molecular motion from momentum transfer dependence of the QENS, illustrated by three different jump models corresponding to C_2, C_3, and C_4 rotations of the same hypothetical molecule. Gray squares represent hypothetical data at discrete values of Q from one sample at fixed temperature. Different jump models can be challenging to discriminate without a sufficient Q range. (*d*) Schematic illustration of incoherent elastic scattering as a function of momentum transfer, $S_{inc}(Q, \omega = 0)$, used to extract the neutron scattering cross-section-weighted atomic mean squared displacement, $\langle u^2 \rangle = 0.5$ Å^2. Gray squares represent hypothetical data at discrete values of Q from one sample at fixed temperature. (*e*,*f*) Dielectric function, ε, including the real (*solid line*), imaginary (*dashed line*), and $\Im(-1/\varepsilon)$ (*dotted line*) components of (*e*) $CH_3NH_3PbI_3$ (41, 42) at 298 K versus (*f*) molecular, liquid H_2O at 298 K (43) and paraelectric ceramic $BaTiO_3$ at 1,000 K (44). The frequency-dependent dielectric function highlights contributions from either molecules (*beige*) or phonons (*lavender*), as detectable by neutron scattering (panel *a*) .

with symmetry-lowering phase transitions on cooling from a paraelectric phase (46), the phonons related to these phase transitions contribute a significant dielectric response, as in the case of $BaTiO_3$ (**Figure 2*f***). Perovskite halides undergo similar symmetry-lowering phase transitions involving changes to the octahedral tilting upon cooling, which relate to soft phonon modes (47–49). Significant entropy releases accompany these canonical phase transitions (50), related to the loss of orientational degrees of freedom of the organic molecule within the changing shape of the nominally cuboctahedral *A*-site void (51–54).

These same collective dynamics influence charge transport primarily through electron–phonon coupling. The optical phonons generate just over half of the polarizability in the dielectric response of $CH_3NH_3PbI_3$, as shown in **Figure 2*e***. In halide perovskites, electron–phonon scattering via the Fröhlich interaction (55) limits the mobility of both free carriers and excitons; therefore, the Fröhlich interaction is the most important form of electron–phonon coupling (14–16). The magnitude of the Fröhlich interaction in $CH_3NH_3PbI_3$ [$\alpha = 1.7$–2.4 (18)] derives predominantly from an ∼11-meV longitudinal optic phonon (**Figure 2*e***) and compares with that of other halide semiconductors, such as TlBr ($\alpha = 2.05$). This value contrasts with the smaller coupling constants of diamond-lattice, tetrahedral semiconductors GaAs ($\alpha = 0.068$) and CdTe ($\alpha = 0.39$) (17, 42).

Fröhlich interaction: coupling of a charge to the presence of the electric field generated from a longitudinal optical phonon

Lone-pair electrons: The ns^2 valence electrons on *B* can be stereochemically activated to create space-filling lone-pair electrons similar to those of NH_3

Plastic crystals: characterized by a lack of orientational order with preservation of translational order

2.2. Independent, Aperiodic Dynamics

In addition to collective motions quantized as phonons, hybrid halide perovskites exhibit more localized, aperiodic motions of both the metal–halide framework and the organic molecules.

2.2.1. Inorganic dipolar dynamics. The fluctuations of lone-pair electrons (56) modify the structure and properties of hybrid perovskites. They have been linked to many exciting aspects of hybrid perovskites, including the large ionic dielectric responses, light holes, and unconventional bandgap: All contribute to the favorable electronic transport and defect tolerance (57). The behavior of these inorganic dipoles (58) resembles that of plastic crystals with permanent, molecular dipoles [e.g., potassium cyanide (7, 59, 60)], but with dynamics on a fast 10^{14}-Hz timescale rather than the slower $\sim 10^{12}$-Hz timescale that is associated with the ionic dynamics shown in **Figure 2*e*,*f***.

All-inorganic perovskites exhibit significant polar dynamics from anharmonic ionic fluctuations, attributed to a head-to-head motion of cesium ions (61). Such polar fluctuations and deformations of the [BX_6] octahedra have been implicated in the formation of polarons, which screen excited-state charge carriers that increase the excited-state lifetimes (62, 63). This explains how all inorganic halide perovskites yield comparable transient electronic responses and device performance to their "hybrid" relatives (64).

2.2.2. Organic cation dynamics. Hybrid halide perovskites are plastic crystals, and the dynamically disordered organic cations impart new degrees of freedom relative to conventional compound semiconductors. These dynamics play a role in various functional properties, deriving primarily from their polarizability (65). Nearly half of the static dielectric polarizability of $CH_3NH_3PbI_3$ derives from the dynamic molecules, akin to that of a polar solvent such as water (**Figure 2*e*,*f***). This polarizability has several implications for charge transport, summarized in **Figure 1*c*** and described below.

Although the exact mechanism behind the long excited-state lifetimes for thermalized and hot carriers remains debated, the orientational dynamics of the organic molecules play an important role in many (and not mutually exclusive) hypotheses. Organic cation dynamics have been implicated in the formation of large polarons that interact with both exciton (66) and free charge carriers (67, 68). The presence of dynamic organic cations accelerates the polaron formation

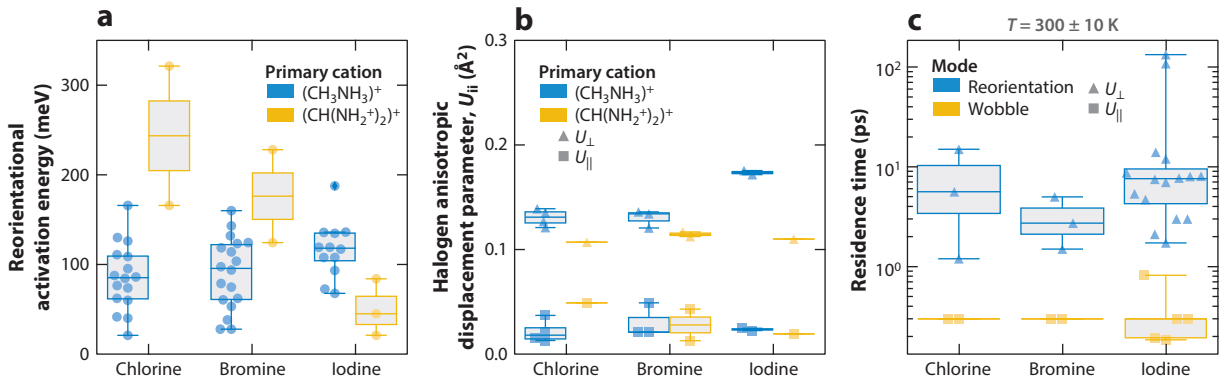

Figure 3

Distribution of activation energies and residence times for organic cation dynamics in $APbX_3$ phases, as differentiated by halogen (A = methylammonium, formamidinium; X = Cl, Br, I). (*a*) Activation energies for molecular reorientational motion further differentiated by organic cation, illustrated by box plots and swarms of individual data points. (*b*) Anisotropic displacement parameters (ADPs) of halogen positions in cubic unit cells ($Pm\bar{3}m$) further differentiated by organic cation, illustrated by box plots and swarms of individual data points. The ADPs are separated into those perpendicular to ($U_\perp$) and parallel to ($U_\parallel$) the Pb–X bonds. (*c*) Residence times at $T = 300 \pm 10$ K for either reorientational (e.g., whole-molecule tumble) or wobble (e.g., C_3 rotation about a C–N axis in methylammonium) motions, including methylammonium- and formamidinium-based phases in their tetragonal and cubic phases. Box plots illustrate the median (*horizontal lines*) and mean (*box center*), while the markers illustrate data points. Data compiled from multiple references are tabulated in the Supplemental Material (39, 47, 51, 53, 73–85).

Supplemental Material >

time [0.3 ps in $CH_3NH_3PbBr_3$ versus 0.7 ps in $CsPbBr_3$ (69)], which extends the lifetime of hot carriers (70). The coupling of inorganic lattice distortions and organic cation reorientations has been shown to screen charge carriers and excitons (13, 14). For example, the lack of interactions between independently reorienting molecules yields a low vibrational group velocity and, thus, poor thermal conductivity with a high heat capacity—an ideal recipe for a phonon bottleneck, in which energetic carriers cannot thermalize efficiently with the lattice due to poor heat removal, as detected by pump-probe spectroscopy experiments (19, 71, 72) and supported by a polaron model backed by density functional theory calculations (68).

Furthermore, the presence of polar fluctuations has the potential to locally and transiently break inversion symmetry of the bulk crystal. Given the slow orientational timescale of the organic dynamics (~5–15 ps) (**Figure 3**) relative to electronic dynamics, it has been proposed that Rashba spin-split valence bands can give rise to direct bandgap-like efficient optical absorption transitions (21, 86–88); carrier thermalization leads to shifted momenta, resulting in indirect-like recombination and longer lifetimes (**Figure 1*c***). Experiments have concluded that the halide perovskites can support static (89, 90) and dynamic (91–94) Rashba spin splitting, with recent evidence that the static effect persists only at low temperatures in hybrids and that both all-inorganic and hybrid materials host a dynamic Rashba effect at room temperature (95). The dynamic Rashba effect appears to originate from anharmonic, polar thermal fluctuations of the inorganic octahedra that may arise from lone-pair electron activity and their interactions with organic cation reorientations or cesium motions (61–63, 95). Therefore, the interplay between organic- and inorganic-centered dynamics has the potential to influence the electronic excited-state dynamics.

The dynamic organic molecules also influence ionic transport and diffusion. Hybrid halide perovskites have a significant ionic contribution to conductivity under various circumstances (23, 25, 96, 97), including under light illumination (24). While ion motion leads to device hysteresis (23), phase separation (98), and decomposition (24), motion of the halogens can lead to the creation

of short-lived electronic defects. Such rapid defect creation can result in defect densities above the thermodynamic limit with sufficiently short lifetimes as to be benign to carrier scattering (99), a finding that is further supported by the self-elimination of intrinsic defects on cooling (100). Furthermore, the timescale of defect motion is faster in hybrid perovskites, as illustrated by the relatively fast self-healing of $CH_3NH_3PbBr_3$ and $CH(NH_2)_2PbBr_3$ from laser-induced defects relative to $CsPbBr_3$ (22). While this fast self-healing leads to a high tolerance for unintentional defects, it makes controlled doping very challenging.

Given the importance of reorientational dynamics in hybrid perovskites for their functional performance, many studies have sought to understand the nature of these dynamics, both of simple hybrid halide perovskites and of technologically relevant complex alloys (101). The remainder of this review describes several case studies of organic cation dynamics through neutron scattering and complementary techniques.

3. CASE STUDIES OF HYBRID PEROVSKITE SEMICONDUCTORS

Myriad competing interactions govern the complex dynamics in hybrid perovskites. The activation energies and residence times of the reorientations of organic cations for several $A\mathrm{Pb}X_3$ perovskites shown in **Figure 3** reflect several trends in ionic size and hydrogen bonding strength. In phases where reorientational dynamics are present (e.g., tetragonal and cubic) (**Figure 3*a***), the activation energy of that motion shows distinct trends for each organic cation. In methylammonium perovskites, the activation energy stays relatively constant as a function of halogen, which correlates more strongly with the constant energy of hydrogen bonding across the halogen series (0.26–0.27 eV/cell) (102) than with the changing size of the halogen (**Figure 1**). However, the nature of the halogen does influence the reorientational barrier in formamidinium perovskites, where the increasing size of the halogen leads to an increased cuboctahedral void size to allow for less inhibited molecular reorientations. This also follows the expected trend in hydrogen bonding strength: 0.16 eV/cell for chlorine, 0.1 eV/cell for bromine, and 0.09 eV/cell for iodine (102). The smaller size of methylammonium decreases the importance of the cuboctahedral void size; the stronger dipole moment of methylammonium yields a higher contribution of hydrogen bonding to the total energy (102). However, the activation energy for methylammonium reorientations increases for iodine, which correlates with an increase in the crystallographic atomic displacement parameter of iodide perpendicular to the Pb–*X* bond that dynamically decreases the cuboctahedral void size (**Figure 3*b***).

Additional complexity is apparent upon examination of the residence times of organic molecules. For both methylammonium and formamidinium perovskites, studies reveal two characteristic residence times for two distinct motions identified as a long-timescale reorientation and a short-timescale wobble (~17 ps and ~0.33 ps, respectively) (**Figure 3*c***). These data demonstrate the composition-dependent interplay of hydrogen bonding and steric interactions on each reorientational mode.

In this section, we present case studies of organic cation dynamics based on neutron spectroscopy and complementary techniques [e.g., nuclear magnetic resonance (NMR), dielectric spectroscopy, time-resolved vibrational spectroscopy], as well as their dependence on chemical substitution and their relationships with optoelectronic properties. These case studies demonstrate the insight that neutron scattering has to offer for hybrid halide perovskites.

3.1. Unsubstituted Hybrid Halide Perovskites

Methylammonium and formamidinium lead halide perovskites are the archetypal members of this family and present complex dynamics essential to understanding substituted materials found in applications and devices.

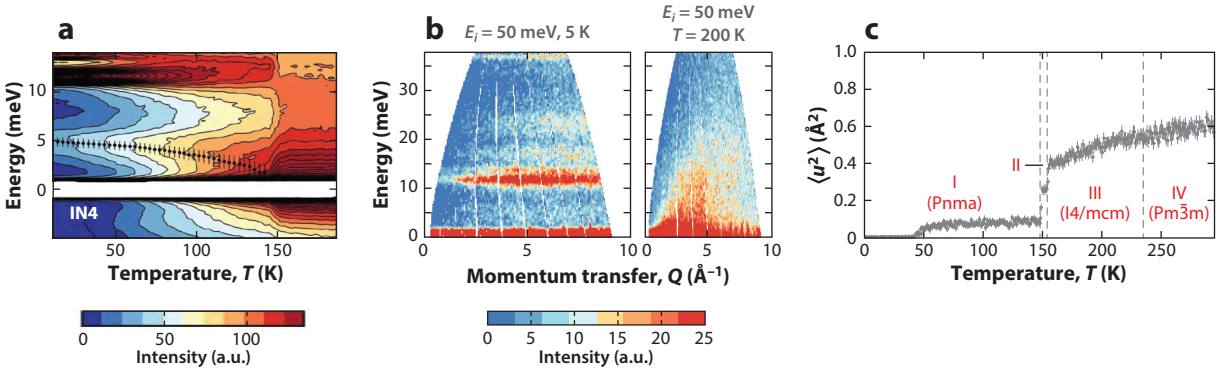

Figure 4

(*a*) Inelastic neutron scattering (*Q* integrated and powder averaged) collected on the IN4 spectrometer from $CH_3NH_3PbBr_3$, showing softening of an ∼5-meV phonon as well as the replacement of an ∼11-meV vibrational mode with a broad, quasi-elastic relaxation above the orthorhombic-to-tetragonal phase transition. (*b*) Inelastic neutron scattering as $S(Q, \omega)$ from powder $CH_3NH_3PbBr_3$, showing the significant overdamping of modes at $T = 200$ K. The sharp, harmonic modes are replaced by quasi-elastic fluctuations extending up to high energies. (*c*) Mean squared displacement of $CH_3NH_3PbBr_3$, $\langle u^2 \rangle$, extracted from an elastic window scan as a function of temperature, showing significant changes in hydrogen dynamics at the tetragonal-to-orthorhombic phase transition, as well as below $T \approx 50$ K. Figure adapted with permission from Reference 47, copyright 2015 American Physical Society.

3.1.1. Methylammonium lead halide perovskites. Methylammonium lead halide perovskites have been the archetypal hybrid perovskite for solar applications, due to the advantageous bandgap of methylammonium lead iodide and the ease of preparation of methylammonium lead iodide compared with the cesium and formamidinium analogs (2, 103, 104). Early NMR and calorimetric studies demonstrated that methylammonium is dynamically disordered in the high-temperature cubic phase, with increased orientational ordering on cooling that relates to the two known phase transitions (105). Between 400 K and 100 K, methylammonium lead iodide transitions from the high-temperature cubic phase (space group: $Pm\bar{3}m$) to a tetragonal phase (space group: I4/mcm) characterized by out-of-phase octahedral rotations when looking perpendicular to the *c* axis (Glazer notation: $a^0a^0c^-$), and then to an orthorhombic phase (space group: Pnma) characterized by additional octahedral tilt axes (Glazer notation: $a^-b^+a^-$) (105). These transitions change the shape and size of the cuboctahedral void where methylammonium sits and, thus, its dynamical behavior.

The phase behavior of $CH_3NH_3PbX_3$ perovskites reflects the presence of organic–inorganic coupling. The phonon dispersion measured in the cubic phase of methylammonium lead iodide with high-energy resolution inelastic X-ray scattering revealed large-amplitude and anharmonic zone-edge rotational instabilities of the octahedra and short-range disorder of the octahedra (48). This disorder is largest for the hybrids, as opposed to all-inorganic materials (106). Subsequent neutron scattering revealed that these instabilities are resolution limited in energy, and thus correspond to static (i.e., with lifetime of $\tau > 36$ ps) tetragonal domains similar to the critical scattering observed from $SrTiO_3$ (49). First-principles calculations reveal that these instabilities are strongly coupled to the librations and reorientations of methylammonium (48).

In $CH_3NH_3PbBr_3$, there is a clear correlation between the phonons of the lead bromide framework and methylammonium dynamics. At the orthorhombic-to-tetragonal order–disorder transition, sharp modes attributed to methylammonium vibrations decrease in scattered amplitude while heating; at the transition these modes are replaced by broad QENS associated with methylammonium reorientation (**Figure 4*a***). The decrease in vibrational mode scattering amplitude accompanies the softening of an ∼5-meV optical phonon from the lead bromide

framework. Furthermore, the tetragonal-phase phonons become strongly overdamped when the organic cations become significantly dynamic (**Figure 4*b***). In $CH_3NH_3PbCl_3$, one observes overdamping of the framework phonon modes across the same temperature scale, as observed with bromine, but without the order–disorder phase transition (107).

Given the significance of hydrogen bonding in $CH_3NH_3PbX_3$ (102), the organic–inorganic interactions are a likely source of anharmonic behavior, as supported by density functional theory calculations of the rotational energy barriers (81). Organic–inorganic coupling in the form of so-called nodding donkey modes are observed in Raman and IR spectroscopy experiments and density functional theory–based calculations thereof (108, 109). The vacancy-ordered double perovskites that lack covalent connectivity between octahedra [e.g., $(CH_3NH_3)_2SnI_6$] also show anharmonic tilting behavior that is correlated with the presence of organic cations (110). Understanding this anharmonicity, and its origins in the organic cation dynamics, is important for describing locally broken symmetries as well as the nature of electron–phonon coupling beyond the linear response (111).

Methylammonium rapidly reorients in the high-temperature cubic phase and exhibits a decrease in amplitude, timescale, and dynamic degrees of freedom on cooling as the cuboctahedral void constricts, as demonstrated by extensive neutron scattering and complementary NMR spectroscopy studies. In methylammonium lead bromide, the temperature-dependent MSDs calculated from incoherent elastic neutron scattering (47) (**Figure 4*c***) capture the overall decrease in motion. The lack of anomalies in $\langle u^2 \rangle$ at the cubic-to-tetragonal phase transition suggests that the entropy loss associated with this phase transition [8.2 J/(mol·K), $\approx R\ln(2.7)$ (51)] correlates to a change in the type of motion rather than to a reduction in the spatial extent of methylammonium dynamics, $\langle u^2 \rangle$. In contrast, the clear feature in the MSD at the tetragonal-to-orthorhombic phase transition suggests a discontinuous change in how methylammonium reorients in the cuboctahedral void. These observations are also consistent with the conservation of ^{1}H and ^{14}N NMR line shapes across the cubic-to-tetragonal phase transition and appreciable narrowing after the tetragonal-to-orthorhombic phase transition (74, 82).

The reorientational dynamics of methylammonium are well described by a jump model of transitions between idealized orientations, as originally suggested by changes in degrees of freedom at various phase transitions determined from calorimetry (51). A rigorous group theoretical analysis by Chen et al. (73) with a jump model provided a complete description of the QENS data (**Figure 5**). This jump model involves the direct product of a C_3 rotation (120°) derived from the internal symmetry axis of methylammonium and a C_4 rotation (90°) perpendicular to the C_3 rotation as imposed by the symmetry of the lattice site point group symmetry. Both the C_3 and C_4 modes are active in the cubic and tetragonal phases, with relaxation times of ~1 ps and ~5 ps, respectively, as determined by two different studies (73, 80). This analysis of the QENS is consistent with direct measurements of the molecular dynamics; two-dimensional transient IR spectroscopy also reveals the presence of a fast (300-fs) wobbling-in-a-cone motion similar to the C_3 rotation and a slow (3-ps) molecular reorientation similar to the C_4 rotation (39).

The molecular reorientations correlate most strongly to the dielectric response. As shown in **Figure 5*b***, the C_4 motion increases significantly in relaxation time on cooling within the tetragonal phase, but this reorientation is frozen out upon cooling into the orthorhombic phase. Therefore, loss of the C_4 reorientation leads to a significant decrease in the dielectric function (41, 53, 105, 112, 113), schematically depicted in **Figure 2**.

Through this organic–inorganic coupling, the dynamic degrees of freedom of methylammonium correlate with changes in the optoelectronic properties. For example, the freezing out of the C_4 whole molecular reorientation at the tetragonal-to-orthorhombic phase transition correlates with faster recombination of excited-state charge carriers as well as with an increase in exciton

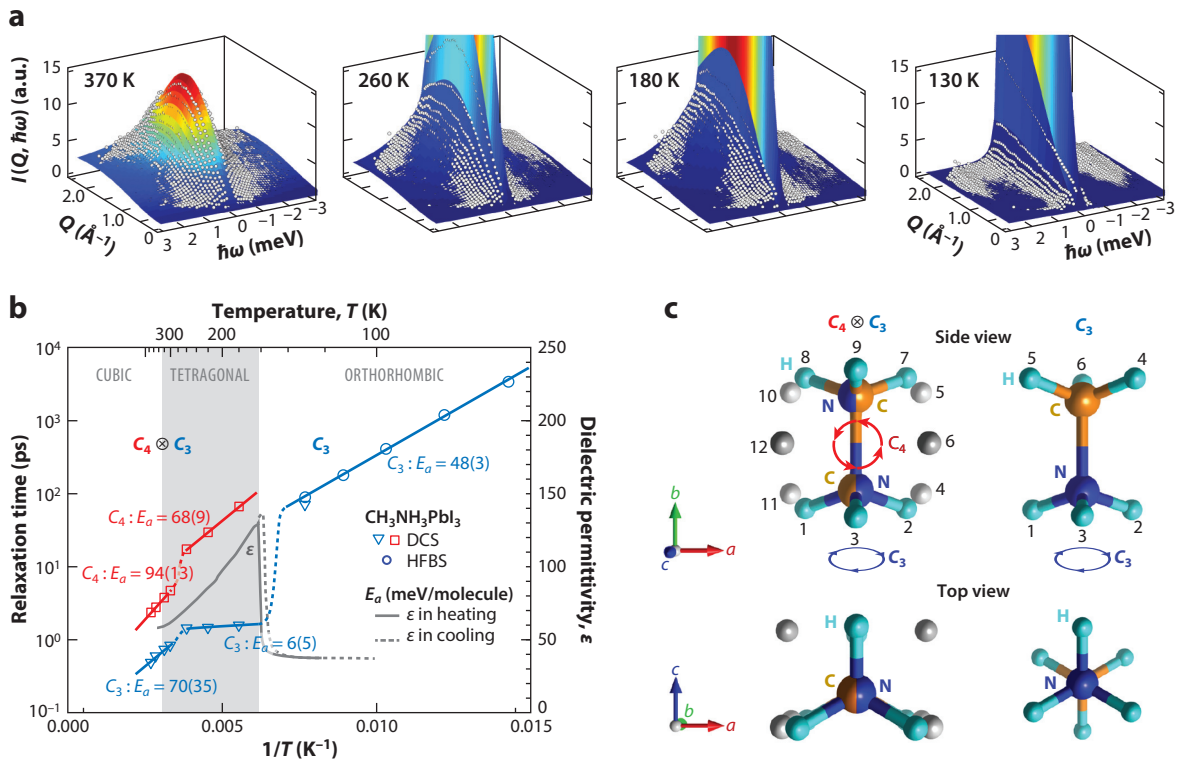

Figure 5

(*a*) Quasi-elastic neutron scattering (QENS) from $CH_3NH_3PbI_3$. Neutron scattering intensity is shown as a function of momentum (Q) and energy ($\hbar\omega$) transfers, measured at 370 K, 260 K, 180 K, and 130 K. Open circles represent the data, and the color-coded surface is the surface image of the calculated jump model. (*b*) Relaxation time, τ, of rotational modes of $CH_3NH_3PbI_3$ obtained from fitting QENS data at various temperatures and plotting them against inverse temperature ($1/T$). The colored solid lines represent the fits to $\ln(\tau) = E_a/(k_B T) - \ln(A)$, where E_a is an activation energy in units of meV per molecule, k_B is the Boltzmann constant, and A is a preexponential factor. The colored dotted lines are guides for the eye. The gray solid and dotted lines represent temperature-dependent dielectric permittivity measured at 1 kHz by Onoda-Yamamuro et al. (53), showing a sharp increase at 160 K. (*c*) $C_3 \otimes C_4$: 12 crystallographically equivalent sites for H atoms of $CH_3NH_3^+$ in the tetragonal environment. C_3: 3 equivalent H atomic sites in the orthorhombic environment. Abbreviations: DCS, disc chopper spectrometer; HFBS, high-flux backscattering spectrometer. Figure adapted with permission from Reference 73, copyright 2015 Royal Society of Chemistry.

binding energies (114, 115). These correlations suggest that the methylammonium C_4 reorientations participate in the electron–phonon models depicted in **Figure 1**.

3.1.2. Formamidinium lead halide perovskites. Formamidinium lead halide perovskites typically have unusual phase behavior in comparison to methylammonium and cesium analogs, including reentrant phase transitions (116), path-dependent phase transitions (104), and crystallographically unresolvable phase transitions (76). Similar to methylammonium perovskites, formamidinium lead halide perovskites exhibit dynamic degrees of freedom within the organic sublattice that freeze out with temperature, which is reflected in the temperature dependence of the dielectric permittivity (75, 76, 113, 116). Anomalies in the temperature-dependent permittivity also occur at phase transition temperatures. Despite these similarities with methylammonium perovskites, the distinct molecular shape and delocalized cationic π system yield several distinctions in formamidinium perovskites.

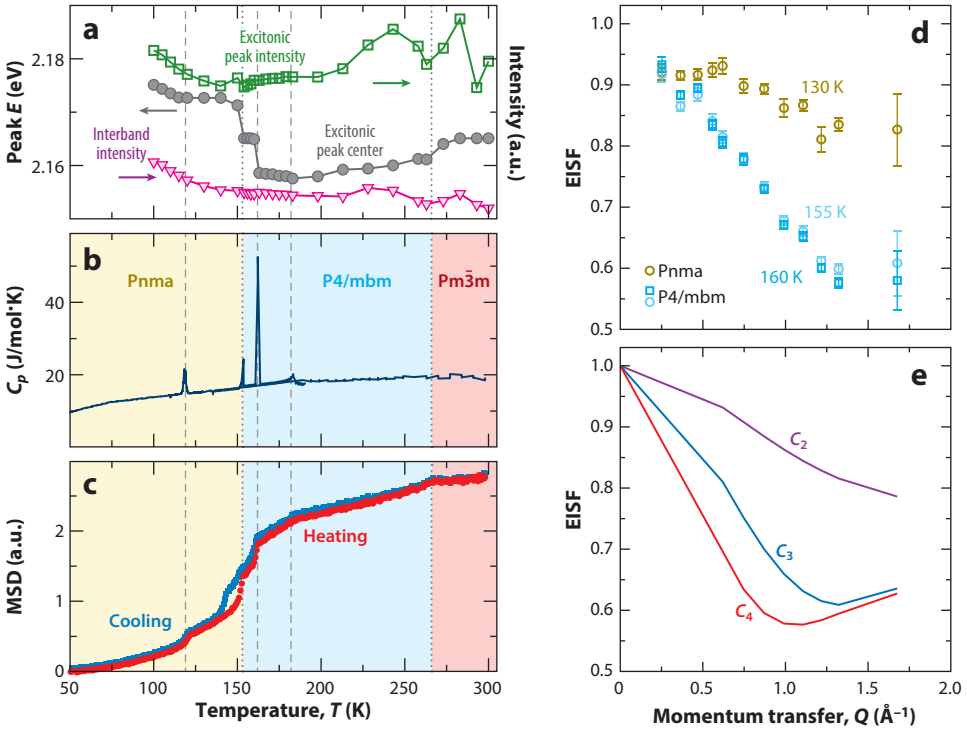

Figure 6

(*a*) Parameters from modeling the temperature-dependent photoconductivity of $CH(NH_2)_2PbBr_3$. Excitonic peak center (*left axis*, *gray circles*), excitonic peak intensity (*right axis*, *green squares*), and interband intensity (*right axis*, *pink triangles*). (*b*) Heat capacity data for $CH(NH_2)_2PbBr_3$. The crystallographically observed phase transitions occur at 266 K and 153 K. (*c*) Mean squared displacements (MSDs) determined from fixed-window elastic neutron scattering of $CH(NH_2)_2PbBr_3$ measured on heating (*red circles*) and cooling (*blue squares*). The colored rectangular overlays in panels *b* and *c* illustrate the crystallographic symmetry at each temperature, with dotted gray lines indicating the crystallographic phase transition temperatures and dashed gray lines showing other phase transition temperatures determined from heat capacity and differential scanning calorimetry data. (*d*) Elastic incoherent structure factors (EISFs) extracted from quasi-elastic neutron scattering spectra at $T = 160$ K, 155 K, and 130 K. (*e*) Models of C_2, C_3, and C_4 molecular rotations shown for comparison. Figure adapted with permission from Reference 76, copyright 2019 American Chemical Society.

Formamidinium lead bromide is notable for having five temperature-dependent anomalies in the MSDs that correlate with anomalies in heat capacity and photoconductivity (76) (**Figure 6**), as well as thermal expansion from dilatometry (117). Two of these phase transitions correspond to changes in crystallographic symmetry, with detectable changes in the octahedral tilting and rotation patterns (76, 118). The remaining three phase transitions release entropy but do not correlate with a readily detectable change in crystallographic symmetry (76, 78, 117). Instead, they are characterized by changes in the dynamic degrees of freedom of formamidinium. As of early 2021, these crystallographically unresolvable phase transitions are unique among hybrid perovskites, although formamidinium lead iodide shows unusual, sample history–dependent phase transitions that are either reentrant and/or entropy stabilized (104, 116).

Based on the molecular geometry, the natural rotations for formamidinium are 180° rotations with the axis of rotation parallel to the carbon–hydrogen bond or about the axis connecting the two nitrogen atoms, as well as a 120° rotation orthogonal to the molecular plane (**Figure 1*a***).

Nuclear quadrupolar resonance (NQR): a nuclear resonance technique performed in the absence of a magnetic field on solids containing quadrupolar nuclei, wherein the nuclear spin levels are split by the local chemical environment and interrogated with radio waves

The point group symmetry of the ideal lattice site occupied by formamidinium suggests that the molecule could undergo reorientational C_4 rotations. Molecular dynamics simulations and density functional theory calculations predict that C_2 rotations, where the axis of rotation connects the two nitrogen atoms rather than a higher symmetry location, are the lowest-energy molecular dynamics (75, 119); these simulations also suggest the presence of a slow reorientation and a fast reorientation, in analogy to those observed in methylammonium perovskites (119). However, direct modeling of the experimental inelastic coherent structure factor is complicated by the complex orientational potential energy landscape of formamidinium within the nearly cuboctahedral void. The EISF resembles a motion between idealized C_3 (120°) and C_4 (90°) rotations at elevated temperatures but 180° rotation at lower temperatures (**Figure 6*e***), consistent with changes in the relaxation times marked by the reduction in QENS peak width across phase transitions (76).

The complex behavior of formamidinium dynamics appears to be related to its distinct distribution of electrostatic charges. Formamidinium has a weaker dipole moment and stronger quadrupole moment than methylammonium (120). A pair of molecular quadrupoles embedded in a dielectric crystal prefer to orient perpendicular to each other in a T shape (121), which can couple strongly to compressive and expansive strains from the surrounding anionic lattice (78). This pairwise T shape cannot tile on any Bravais lattice; therefore, the molecular orientations of formamidinium are frustrated (76). Frustrated orientations are consistent with NMR results showing that formamidinium reorients more quickly than methylammonium and with dielectric susceptibility measurements that indicate a series of complex changes in formamidinium dynamics at low temperatures (118, 122). This geometric frustration participates in the orientational phase transitions of formamidinium lead bromide observed with QENS and could explain the path-dependent phase transitions of formamidinium lead iodide. ^{79}Br nuclear quadrupolar resonance (NQR) data suggest that the reorientations of formamidinium couple to changes in the local environment around the inorganic octahedra, aligning with first-principles calculations showing that the rotational energy barrier of formamidinium can be tuned with substitution on the halide and metal sites (78, 123). Understanding the unusual phase behavior of formamidinium perovskites is essential to understanding their properties, as each phase has a different optoelectronic behavior (76, 116).

3.1.3. Lead-free hybrid halide perovskites. While more difficult to experimentally study (e.g., due to air sensitivity), tin and germanium perovskites offer new opportunities for functional properties, as they show an increased contribution from ns^2 lone-pair electrons and lack the toxicity of lead (57, 124, 125). The increased stereochemical activity in tin and germanium perovskites relative to that in lead perovskites (106, 126) is expected to couple to the dynamic degrees of freedom of methylammonium (58), although studies so far have focused predominantly on ionic conductivity (127, 128). However, density functional theory calculations also indicate that tin and germanium perovskites have higher energy barriers for methylammonium reorientations, attributed to a decrease in lattice polarizability and compression of the *A*-site void (81, 129, 130). Furthermore, the overall phase behavior appears to be more sensitive to the molecular dynamics, as isotope enrichment can completely change [e.g., $CH_3NH_3SnBr_3$ (131) versus $CD_3ND_3SnBr_3$ (54)] or suppress phase transitions [e.g., $CH_3NH_3GeCl_3$ versus $CD_3ND_3GeCl_3$ (128)]. Experimental validation of these computational predictions and investigation into lone-pair coupling to methylammonium dynamic degrees of freedom provide exciting avenues for continued research.

3.2. Effects of Chemical Substitution

Most of the technologically relevant hybrid halide perovskites for photovoltaic applications are heavily chemically substituted (i.e., alloyed), as exemplified by a high-performing composition:

$(CH(NH_2)_2)_{0.79}(CH_3NH_3)_{0.16}Cs_{0.05}Pb(I_{0.84}Br_{0.17})_3$ (101). Chemical substitution is easily accomplished synthetically in the solution-phase or solid-state route to these materials (101, 132), which enables tuning of optoelectronic properties such as the bandgap and polaron mobility (27, 133). Furthermore, the unsubstituted hybrid perovskites methylammonium lead iodide and formamidinium lead iodide are enthalpically unstable (29) and decompose rapidly under ambient conditions (134–137); certain substitutions stabilize the perovskite phases (138) or slow this decomposition process (101, 139, 140). While chemical substitution can improve phase stability, it modifies the internal energy landscape of hybrid perovskites, which influences the atomistic dynamics and, thus, electron–phonon coupling (27, 141).

This section focuses on the role of cesium substitution in the two perovskite materials described above, methylammonium lead bromide and formamidinium lead bromide. In contrast to the hybrid materials, cesium lead bromide exhibits orthorhombic symmetry with octahedral tilting at and below room temperature, with the cubic and tetragonal phases accessible at temperatures above 80°C and 140°C, respectively (142). The generalized phase behavior of the substituted alloys can be understood within the context of a pseudobinary phase diagram, where compositions closest to the end members behave as solid solutions separated by a two-phase region for intermediate compositions. However, the detailed nature of the phase transitions requires closer examination of the dynamic nature of the organic cations in these plastic crystals.

3.2.1. Cesium substitution in methylammonium lead bromide. In methylammonium lead bromide, cesium substitution for methylammonium leads to inhibition of the methylammonium dynamics. As discussed above, methylammonium undergoes 90° rotations perpendicular and 120° rotations parallel to the carbon–nitrogen bond axis (73). Substitution of cesium for methylammonium in the solid solution, $(CH_3NH_3)_{1-x}Cs_xPbBr_3$, does not affect the identity of these rotations; however, modeling of the QENS spectra demonstrates that a fraction of molecules become pinned as the concentration of cesium increases (77) (**Figure 7*a–c***). As discussed above, the molecular reorientations are directly responsible for a significant fraction of the increased dielectric polarizability (**Figure 5*b***).

The pinning of molecular reorientations with a cesium substitution in $(CH_3NH_3)_{1-x}Cs_xPbBr_3$ correlates with a significant modification of the phase behavior. In contrast to $CH_3NH_3PbBr_3$ (**Figure 4**), the temperature-dependent MSDs vary smoothly with temperature and do not show abrupt changes near crystallographic phase transition temperatures in the substituted materials (77) (**Figure 7**). Crystallography indicates that, with increasing substitution, the phase transitions occur over a wider temperature range and are dependent on temperature ramp rate (77). The sluggish phase transitions and inhibited dynamics indicate that methylammonium lead bromide becomes an orientational glass upon cesium substitution characterized by disordered and frozen methylammonium orientations, similar to bromide substitution in potassium cyanide (59).

In analogy to spin glasses, the formation of an orientational glass involves frustration of order parameters related to the orientation of the molecule (59). A possible reason for the increased frustration on substitution is that cesium and methylammonium prefer different coordination within the octahedral framework. Most halide perovskites crystallize in the tetragonal P4/mbm phase, characterized by in-phase octahedral rotations, as this configuration maximizes *A*-site coordination (143). Hydrogen bonding interactions between methylammonium and the octahedral framework cause methylammonium perovskites to prefer the tetragonal I4/mcm phase, characterized by out-of-phase octahedral rotations (144–146). These interactions, combined with the contraction of the *A* site with cesium substitution, compete and lead to the inhibition of methylammonium reorientations and the formation of an orientational glass. It appears that substitution increases

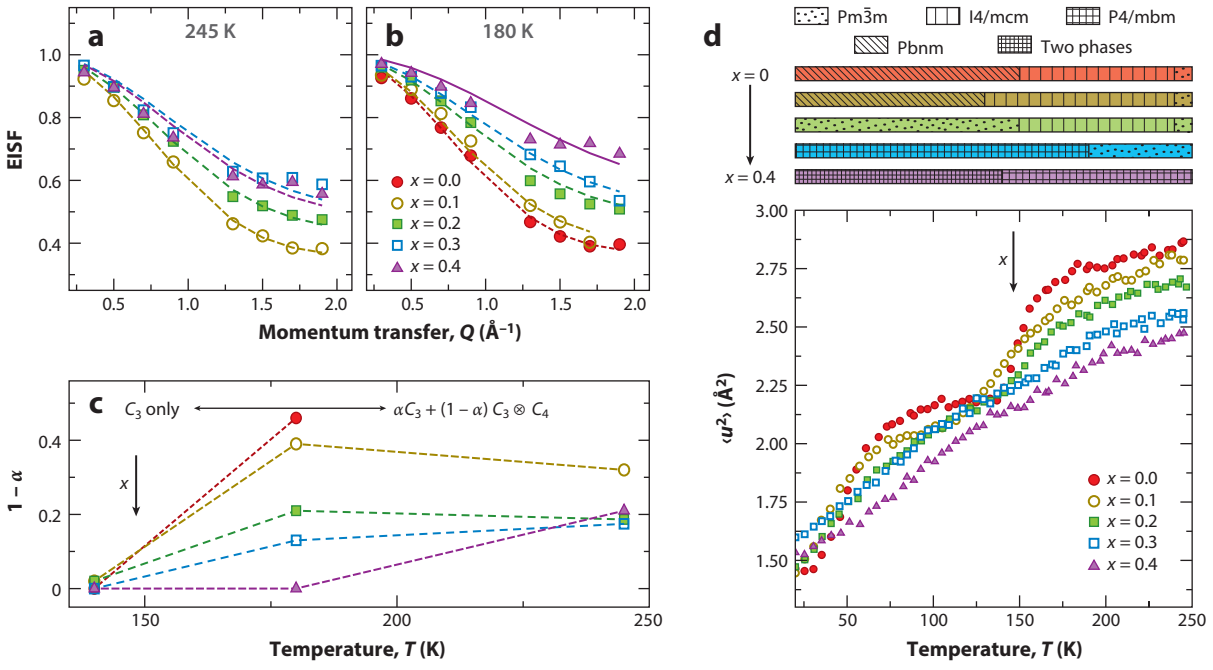

Figure 7

Selected elastic incoherent structure factor (EISF) values for $(CH_3NH_3)_{1-x}Cs_xPbBr_3$ extracted from quasi-elastic neutron scattering (QENS) spectra collected at (*a*) 245 K and (*b*) 180 K. The dashed lines represent fits to the coupled C_3 and C_4 jump model, and the solid lines represent fits to the C_3 jump model. (*c*) The fraction of $CH_3NH_3^+$ participating in a $C_3 \otimes C_4$ rotation $(1-\alpha)$ from the EISF modeling. The dashed lines are guides for the eye. (*d*) Mean squared displacements as a function of temperature extracted from QENS spectra of $(CH_3NH_3)_{1-x}Cs_xPbBr_3$, illustrating a smearing of transitions with increasing x. The bars at the top illustrate the observed lattice symmetry of $(CH_3NH_3)_{1-x}Cs_xPbBr_3$ for $x = 0.0$, 0.1, 0.2, 0.3, and 0.4. Figure adapted with permission from Reference 77, copyright 2017 American Chemical Society.

the influence of hydrogen bonding (cf. **Figure 3**). Recent first-principles calculations suggest that reductions in symmetry, such as those from frozen or inhibited methylammonium reorientations, change the binding energy of polarons (27) or tune the magnitude of Rashba splitting (141), indicating that substitution influences electronic properties through organic cation dynamics.

3.2.2. Cesium substitution in formamidinium lead bromide. The orientational phase transitions of formamidinium lead bromide are sensitive to chemical substitution. The five phase transitions of formamidinium lead bromide have dynamic signatures that manifest in ^{1}H NMR, ^{14}N NMR, and MSDs between room temperature and 100 K (**Figure 6**). However, formamidinium lead bromide substituted with as little as 5–10% cesium exhibits only one anomaly in ^{1}H NMR, ^{14}N NMR, or MSDs between room temperature and 100 K, which corresponds to the high-temperature cubic-to-tetragonal phase transition (78) (**Figure 8*a***).

Cesium substitution effectively suppresses the four low-temperature phase transitions by interrupting the concerted changes in formamidinium dynamics. At room temperature, ^{14}N NMR spectra of $(CH(NH_2)_2)_{1-x}Cs_xPbBr_3$ show retained reorientational dynamics, but with an increased anisotropy of the ^{14}N environment with x; the anisotropy accompanies a clear distortion of the local ^{79}Br environments, as determined by NQR spectroscopy (**Figure 8*b***). The interplay between substitution and formamidinium orientation reflects a behavior distinct from that of methylammonium (**Figure 3**), which can be linked to the large electrostatic quadrupolar

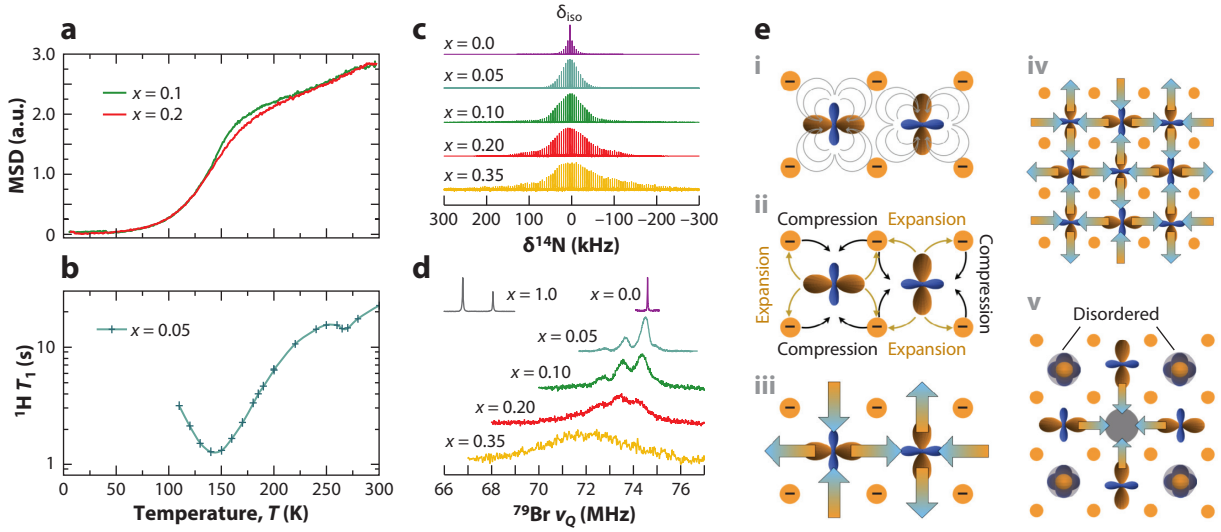

Figure 8

(*a*) Mean squared displacements (MSDs) extracted from fixed-window elastic neutron scattering spectra for $(CH(NH_2)_2)_{1-x}Cs_xPbBr_3$, where $x = 0.1$ and 0.2, illustrate a lack of discontinuities in substituted samples (in contrast to **Figure 6*c***). (*b*) Spin-lattice relaxation time (T_1) determined from ^{1}H NMR spectroscopy of $(CH(NH_2)_2)_{0.95}Cs_{0.05}PbBr_3$ illustrates one phase transition at $T \sim 260$ K. (*c*) Room-temperature ^{14}N NMR spectra of $(CH(NH_2)_2)_{1-x}Cs_xPbBr_3$, where $x = 0$ to 0.35, illustrate an increased anisotropy of cation rotations with x. (*d*) Room-temperature ^{79}Br NQR spectra collected for $(CH(NH_2)_2)_{1-x}Cs_xPbBr_3$ show that increasing the level of substitution leads to an effectively continuous distribution of possible local environments. (*e*) (*i*, *ii*) Electrostatic potential field lines emanating from the quadrupolar moment of formamidinium (*orange* denotes negative density; *blue* denotes positive density) yield attractive or repulsive interactions to the anionic framework. (*iii*) The resulting expansive and compressive strain fields map onto an elastic dipole tensor (*large arrows*). (*iv*) In a plane, the elastic dipoles can order; however, a favorable three-dimensional configuration cannot be tiled. (*v*) The smaller Cs^+ cation introduces compressive local strain, thereby causing a preferred orientation of quadrupolar cations around the Cs^+ and frustrated orientations of the next-nearest-neighboring quadrupoles. Figure adapted with permission from Reference 78, copyright 2020 American Chemical Society.

moment of formamidinium (**Figure 8*c***). The relative orientations of formamidinium within the inorganic framework are mediated by the electrostatic quadrupolar field, which is very sensitive to the surrounding electric field gradient. When this interaction is mapped onto an elastic dipole tensor, one can see how a stable long-range-ordered configuration becomes challenging to produce (i.e., it is frustrated). Introduction of compressive microstrain from the smaller cesium cation significantly changes the potential energy landscape, with consequences for the long-range order and phase transitions (78). While the long-range order is strongly influenced by the substitution, the local dynamics of formamidinium appear to be mostly retained (78), suggesting that formamidinium-based perovskites serve as a better host for substituted alloys if one wishes to maintain a larger dielectric response.

3.2.3. Complex, multiple substitutions in hybrid halide perovskites. The ability to use a cocktail of cations and anions to create highly stable, functional photovoltaic devices reflects a unique defect tolerance of hybrid perovskites (101). While pseudobinary solid solutions formed by substitution on either the *A* site [e.g., $(CH(NH_2)_2)_{1-x}Cs_xPbI_3$ (147)] or the halogen site [e.g., $CH_3NH_3Pb(I_{1-x}Br_x)_3$ (98)] are prone to phase separation and decomposition, complex, multiple substitutions on both *A* and halogen sites prevent this phase separation (148). The chemical pressure from cesium substitution for methylammonium in $(CH_3NH_3)_{0.5}Cs_{0.5}Pb(Br_{0.5}I_{0.5})_3$ appears

to have the same influence as exerting 0.2 GPa of external pressure on $CH_3NH_3Pb(Br_{0.5}I_{0.5})_3$ and thermodynamically stabilizes the solid solution, highlighting the importance of an often-overlooked $P\Delta V$ term in the thermodynamic potential (149).

Therefore, one expects complex substitutions to also influence the organic molecular dynamics. The inhibition with cesium substitution in methylammonium perovskites resembles that of methylammonium-substituted formamidinium lead iodide, in which line-shape analysis of ^{14}N NMR spectra reveals that methylammonium and formamidinium reorientations become increasingly anisotropic with increased substitution (122). Substitution at the halide site, as has been used to increase stability and tune the electronic bandgap (101, 150), also leads to inhibited cation dynamics. Pump-probe two-dimensional IR spectroscopy studies of $CH_3NH_3Pb(Cl_xBr_{1-x})_3$ and $CH_3NH_3Pb(Br_xI_{1-x})_3$ show that both series exhibit slower methylammonium dynamics than either end member (79). This finding supports the observation of decreased orientational disorder in methylammonium lead bromide after chlorine substitution, as determined by Fourier difference maps from Rietveld refinement of neutron powder diffraction (151). Many of the top-performing photovoltaic devices substitute a formamidinium-based host (1). Given that local formamidinium dynamics are not significantly inhibited by substitution (78), any advantage of having a dynamic organic cation is still active in formamidinium-based materials.

4. CONCLUSIONS AND OUTLOOK

Collective and local dynamics in hybrid perovskites underlie the optoelectronic properties that make them of interest for photovoltaics, radiation detection, and light-emitting diodes. Therefore, characterization of these dynamics is essential for building useful theories to describe their behavior, especially for local dynamics that do not yet have rigorous models. Neutron scattering plays a large role in uncovering these dynamics—the dynamic structure factor, $S(Q, \omega)$, informs researchers of the correlations of these molecular dynamics in both space and time. Complementary methods, such as NMR, dielectric spectroscopies, X-ray scattering, molecular dynamics simulations, and density functional theory calculations, provide a complete perspective across many environmental conditions. Neutron scattering has been used to track changes in molecular dynamics as a function of temperature, to describe the symmetry of molecular reorientations, and to characterize the activation energy of molecular dynamics. These investigations demonstrate that these local dynamics are affected by cation identity, by electrostatic and hydrogen bonding interactions with the extended octahedral framework, and by substitution. This relationship creates a deeper understanding of the phase behavior of hybrid halide perovskites. Investigations into two-dimensional perovskite materials have only just begun, and many questions remain about the dynamic degrees of freedom of bulky organic cations and their relationship to optoelectronic properties. Similar questions remain for other hybrid perovskite derivatives, including zero-dimensional vacancy-ordered perovskites. These insights are the basis of rigorous structure–property relationships that will enable innovations in next-generation semiconductors.

SUMMARY POINTS

1. Hybrid perovskite semiconductors are plastic crystals with dynamically reorienting organic cations.
2. Organic cation dynamics have a direct influence on the dielectric response of hybrid perovskite semiconductors.

3. Molecular reorientational dynamics exert indirect influences on the optical and electronic properties of hybrid perovskites by way of locally broken symmetry, electron–phonon coupling, and defect creation and motion.
4. Chemical substitution of hybrid perovskite semiconductors influences the thermodynamic stability and dynamics of organic cations.

DISCLOSURE STATEMENT

The authors are not aware of any affiliations, memberships, funding, or financial holdings that might be perceived as affecting the objectivity of this review.

ACKNOWLEDGMENTS

The writing of this review was supported by the US Department of Energy, Office of Science, Basic Energy Sciences, under award SC0016083. J.R.N. and E.M.M. also acknowledge support from Research Corporation for Science Advancement through a Cottrell Scholar Award and the A.P. Sloan Foundation for assistance provided from a Sloan Research Fellowship. The authors also thank K.A. Ross and A.E. Maughan for insightful discussions.

LITERATURE CITED

1. Kim JY, Lee JW, Jung HS, Shin H, Park NG. 2020. High-efficiency perovskite solar cells. *Chem. Rev.* 120:7867–918
2. Stranks SD, Snaith HJ. 2015. Metal-halide perovskites for photovoltaic and light-emitting devices. *Nat. Nanotechnol.* 10:391–402
3. Xu Q, Wei H, Wei W, Chuirazzi W, DeSantis D, et al. 2017. Detection of charged particles with a methylammonium lead tribromide perovskite single crystal. *Nucl. Instrum. Methods A* 848:106–8
4. Nazarenko O, Yakunin S, Morad V, Cherniukh I, Kovalenko MV. 2017. Single crystals of caesium formamidinium lead halide perovskites: solution growth and gamma dosimetry. *NPG Asia Mater.* 9:e373
5. Smith MD, Crace EJ, Jaffe A, Karunadasa HI. 2018. The diversity of layered halide perovskites. *Annu. Rev. Mater. Res.* 48:111–36
6. Shannon RD. 1976. Revised effective ionic radii and systematic studies of interatomic distances in halides and chalcogenides. *Acta Crystallogr. A* 32:751–67
7. Staveley LAK. 1962. Phase transitions in plastic crystals. *Annu. Rev. Phys. Chem.* 13:351–68
8. Kieslich G, Sun S, Cheetham T. 2015. An extended tolerance factor approach for organic-inorganic perovskites. *Chem. Sci.* 6:3430–33
9. Megaw HD. 1973. *Crystal Structure: A Working Approach*. Philadelphia: Saunders
10. Mitzi DB. 2001. Templating and structural engineering in organic–inorganic perovskites. *J. Chem. Soc. Dalton Trans.* 2001:1–12
11. Woodward PM. 1997. Octahedral tilting in perovskites. II. Structure stabilizing forces. *Acta Crystallogr. B* 53:44–66
12. Ghosh D, Welch E, Neukirch AJ, Zakhidov A, Tretiak S. 2020. Polarons in halide perovskites: a perspective. *J. Phys. Chem. Lett.* 9:3271–86
13. Even J, Pedesseau L, Katan C. 2014. Analysis of multivalley and multibandgap absorption and enhancement of free carriers related to exciton screening in hybrid perovskites. *J. Phys. Chem. C* 118:11566–72
14. Neukirch AJ, Nie W, Blancon JC, Appavoo K, Tsai H, et al. 2016. Polaron stabilization by cooperative lattice distortion and cation rotations in hybrid perovskite materials. *Nano Lett.* 16:3809–16
15. Herz LM. 2017. Charge-carrier mobilities in metal halide perovskites: fundamental mechanisms and limits. *ACS Energy Lett.* 2:1539–48

16. Even J, Paofai S, Bourges P, Létoublon A, Cordier S, et al. 2016. Carrier scattering processes and low energy phonon spectroscopy in hybrid perovskite crystals. *Proc. SPIE* 9743:97430M
17. Wright AD, Verdi C, Milot RL, Eperon GE, Pérez-Osorio MA, et al. 2016. Electron–phonon coupling in hybrid lead halide perovskites. *Nat. Commun.* 7:11755
18. Miyata K, Atallah TL, Zhu XY. 2017. Lead halide perovskites: crystal-liquid duality, phonon glass electron crystals, and large polaron formation. *Sci. Adv.* 3:e1701469
19. Yang Y, Ostrowski DP, France RM, Zhu K, van de Lagemaat J, et al. 2015. Observation of a hot-phonon bottleneck in lead-iodide perovskites. *Nat. Photonics* 10:53–59
20. Pötz W. 1987. Hot-phonon effects in bulk GaAs. *Phys. Rev. B* 36:5016–19
21. Kim M, Im J, Freeman AJ, Ihm J, Jin H. 2014. Switchable $S = 1/2$ and $J = 1/2$ Rashba bands in ferroelectric halide perovskites. *PNAS* 111:6900–4
22. Ceratti DR, Rakita Y, Cremonesi L, Tenne R, Kalchenko V, et al. 2018. Self-healing inside $APbBr_3$ halide perovskite crystals. *Adv. Mater.* 30:1706273
23. Eames C, Frost JM, Barnes PRF, O'Regan BC, Walsh A, Islam MS. 2015. Ionic transport in hybrid lead iodide perovskite solar cells. *Nat. Commun.* 6:7497
24. Kim GY, Senocrate A, Yang TY, Gregori G, Grätzel M, Maier J. 2018. Large tunable photoeffect on ion conduction in halide perovskites and implications for photodecomposition. *Nat. Mater.* 17:445–49
25. Senocrate A, Moudrakovski I, Kim GY, Yang TY, Gregori G, et al. 2017. The nature of ion conduction in methylammonium lead iodide: a multimethod approach. *Angew. Chem. Int. Ed.* 56:7755–59
26. Wang R, Mujahid M, Duan Y, Wang Z, Xue J, Yang Y. 2019. A review of perovskites' solar cell stability. *Adv. Funct. Mater.* 29:1808843
27. Zhou L, Katan C, Nie W, Tsai H, Pedesseau L, et al. 2019. Cation alloying delocalizes polarons in lead-halide perovskites. *J. Phys. Chem. Lett.* 10:3516–24
28. Deretzis I, Smecca E, Mannino G, La Magna A, Miyasaka T, Alberti A. 2018. Stability and degradation in hybrid perovskites: Is the glass half-empty or half-full? *J. Phys. Chem. Lett.* 9:3000–7
29. Nagabhushana GP, Shivaramaiah R, Navrotsky A. 2016. Direct calorimetric verification of thermodynamic instability of lead halide hybrid perovskites. *PNAS* 113:7717–21
30. Lai M, Obliger A, Lu D, Kley CS, Bischak CG, et al. 2018. Intrinsic anion diffusivity in lead halide perovskites is facilitated by a soft lattice. *PNAS* 115:11929–34
31. Zhang Z, Roy PN, Li H, Avdeev M, Nazar LF. 2019. Coupled cation–anion dynamics enhances cation mobility in room-temperature superionic solid-state electrolytes. *J. Am. Chem. Soc.* 141:19360–72
32. Sun Y, Wang Y, Liang X, Xia Y, Peng L, et al. 2019. Rotational cluster anion enabling superionic conductivity in sodium-rich antiperovskite Na_3OBH_4. *J. Am. Chem. Soc.* 141:5640–44
33. Smith MD, Jaffe A, Dohner ER, Lindenberg AM, Karunadasa HI. 2017. Structural origins of broadband emission from layered Pb-Br hybrid perovskites. *Chem. Sci.* 8:4497–504
34. Gong X, Voznyy O, Jain A, Liu W, Sabatini R, et al. 2018. Electron–phonon interaction in efficient perovskite blue emitters. *Nat. Mater.* 17:550–56
35. Steirer KX, Schulz P, Teeter G, Stevanovic V, Yang M, et al. 2016. Defect tolerance in methylammonium lead triiodide perovskite. *ACS Energy Lett.* 1:360–66
36. Brandt RE, Stevanović V, Ginley DS, Buonassisi T. 2015. Identifying defect-tolerant semiconductors with high minority-carrier lifetimes: beyond hybrid lead halide perovskites. *MRS Commun.* 5:265–75
37. Sears VF. 1992. Neutron scattering lengths and cross sections. *Neutron News* 3:26–37
38. Létoublon A, Paofai S, Rufflé B, Bourges P, Hehlen B, et al. 2016. Elastic constants, optical phonons, and molecular relaxations in the high temperature plastic phase of the $CH_3NH_3PbBr_3$ hybrid perovskite. *J. Phys. Chem. Lett.* 7:3776–84
39. Bakulin AA, Selig O, Bakker HJ, Rezus YL, Müller C, et al. 2015. Real-time observation of organic cation reorientation in methylammonium lead iodide perovskites. *J. Phys. Chem. Lett.* 6:3663–69
40. Bée M. 1988. *Quasielastic Neutron Scattering*. Boca Raton, FL: CRC. 1st ed.
41. Anusca I, Balčiūnas S, Gemeiner P, Svirskas V, Sanlialp M, et al. 2017. Dielectric response: answer to many questions in the methylammonium lead halide solar cell absorbers. *Adv. Energy Mater.* 7:1700600
42. Sendner M, Nayak PK, Egger DA, Beck S, Müller C, et al. 2016. Optical phonons in methylammonium lead halide perovskites and implications for charge transport. *Mater. Horiz.* 3:613–20

43. Ellison WJ. 2007. Permittivity of pure water, at standard atmospheric pressure, over the frequency range 0–25 THz and the temperature range 0–100°C. *J. Phys. Chem. Ref. Data* 36:1–18
44. Luspin Y, Servoin JL, Gervais F. 1980. Soft mode spectroscopy in barium titanate. *J. Phys. C* 13:3761–73
45. Pelant I, Valenta J. 2012. *Luminescence Spectroscopy of Semiconductors*. Oxford, UK: Oxford Univ. Press
46. Megaw HD. 1952. Origin of ferroelectricity in barium titanate and other perovskite-type crystals. *Acta Crystallogr.* 5:739–49
47. Swainson IP, Stock C, Parker SF, Van Eijck L, Russina M, Taylor JW. 2015. From soft harmonic phonons to fast relaxational dynamics in $CH_3NH_3PbBr_3$. *Phys. Rev. B* 92:100303
48. Beecher AN, Semonin OE, Skelton JM, Frost JM, Terban MW, et al. 2016. Direct observation of dynamic symmetry breaking above room temperature in methylammonium lead iodide perovskite. *ACS Energy Lett.* 1:880–87
49. Weadock NJ, Gehring PM, Gold-Parker A, Smith IC, Karunadasa HI, Toney MF. 2020. Test of the dynamic-domain and critical scattering hypotheses in cubic methylammonium lead triiodide. *Phys. Rev. Lett.* 125:075701
50. Katan C, Mohite AD, Even J. 2018. Entropy in halide perovskites. *Nat. Mater.* 17:377–79
51. Onoda-Yamamuro N, Matsuo T, Suga H. 1990. Calorimetric and IR spectroscopic studies of phase transitions in methylammonium trihalogenoplumbates (II). *J. Phys. Chem. Solids* 51:1383–95
52. Onoda-Yamamuro N, Matsuo T, Suga H. 1991. Thermal, electric, and dielectric properties of $CH_3NH_3SnBr_3$ at low temperatures. *J. Chem. Thermodyn.* 23:987–99
53. Onoda-Yamamuro N, Matsuo T, Suga H. 1992. Dielectric study of $CH_3NH_3PbX_3$ (X = Cl, Br, I). *J. Phys. Chem. Solids* 53:935–39
54. Onoda-Yamamuro N, Yamamuro O, Matsuo T, Suga H, Oikawa K, et al. 1995. Neutron-diffraction study of $CD_3ND_3SnBr_3$: semiconductor–insulator transition with orientational ordering. *Physica B* 213/214:411–13
55. Cardona M, Peter YY. 2005. *Fundamentals of Semiconductors*. Berlin: Springer
56. Walsh A, Payne DJ, Egdell RG, Watson GW. 2011. Stereochemistry of post-transition metal oxides: revision of the classical lone pair model. *Chem. Soc. Rev.* 40:4455–63
57. Fabini DH, Seshadri R, Kanatzidis MG. 2020. The underappreciated lone pair in halide perovskites underpins their unusual properties. *MRS Bull.* 45:467–77
58. Remsing RC, Klein ML. 2020. A new perspective on lone pair dynamics in halide perovskites. *APL Mater.* 8:050902
59. Loidl A. 1989. Orientational glasses. *Annu. Rev. Phys. Chem.* 40:29–60
60. Höchli U, Knorr K, Loidl A. 1990. Orientational glasses. *Adv. Phys.* 39:405–615
61. Yaffe O, Guo Y, Tan LZ, Egger DA, Hull T, et al. 2017. Local polar fluctuations in lead halide perovskite crystals. *Phys. Rev. Lett.* 118:136001
62. Wu X, Tan LZ, Shen X, Hu T, Miyata K, et al. 2017. Light-induced picosecond rotational disordering of the inorganic sublattice in hybrid perovskites. *Sci. Adv.* 3:e1602388
63. Park M, Neukirch AJ, Reyes-Lillo SE, Lai M, Ellis SR, et al. 2018. Excited-state vibrational dynamics toward the polaron in methylammonium lead iodide perovskite. *Nat. Commun.* 9:2525
64. Zhu H, Trinh MT, Wang J, Fu Y, Joshi PP, et al. 2017. Organic cations might not be essential to the remarkable properties of band edge carriers in lead halide perovskites. *Adv. Mater.* 29:1603072
65. Even J, Carignano M, Katan C. 2016. Molecular disorder and translation/rotation coupling in the plastic crystal phase of hybrid perovskites. *Nanoscale* 8:6222–36
66. Thouin F, Valverde-Chávez DA, Quarti C, Cortecchia D, Bargigia I, et al. 2019. Phonon coherences reveal the polaronic character of excitons in two-dimensional lead halide perovskites. *Nat. Mater.* 18:349–56
67. Wolf C, Cho H, Kim YH, Lee TW. 2017. Polaronic charge carrier–lattice interactions in lead halide perovskites. *ChemSusChem* 10:3705–11
68. Frost JM, Whalley LD, Walsh A. 2017. Slow cooling of hot polarons in halide perovskite solar cells. *ACS Energy Lett.* 2:2647–52
69. Miyata K, Meggiolaro D, Trinh MT, Joshi PP, Mosconi E, et al. 2017. Large polarons in lead halide perovskites. *Sci. Adv.* 3:e1701217

70. Zhu H, Miyata K, Fu Y, Wang J, Joshi PP, et al. 2016. Screening in crystalline liquids protects energetic carriers in hybrid perovskites. *Science* 353:1409–13
71. Yang J, Wen X, Xia H, Sheng R, Ma Q, et al. 2017. Acoustic-optical phonon up-conversion and hot-phonon bottleneck in lead-halide perovskites. *Nat. Commun.* 8:14120
72. Monahan DM, Guo L, Lin J, Dou L, Yang P, Fleming GR. 2017. Room-temperature coherent optical phonon in 2D electronic spectra of $CH_3NH_3PbI_3$ perovskite as a possible cooling bottleneck. *J. Phys. Chem. Lett.* 8:3211–15
73. Chen T, Foley BJ, Ipek B, Tyagi M, Copley JRD, et al. 2015. Rotational dynamics of organic cations in the $CH_3NH_3PbI_3$ perovskite. *Phys. Chem. Chem. Phys.* 17:31278–86
74. Bernard GM, Wasylishen RE, Ratcliffe CI, Terskikh V, Wu Q, et al. 2018. Methylammonium cation dynamics in methylammonium lead halide perovskites: a solid-state NMR perspective. *J. Phys. Chem. A* 122:1560–73
75. Fabini DH, Siaw TA, Stoumpos CC, Laurita G, Olds D, et al. 2017. Universal dynamics of molecular reorientation in hybrid lead iodide perovskites. *J. Am. Chem. Soc.* 139:16875–84
76. Mozur EM, Trowbridge JC, Maughan AE, Gorman MJ, Brown CM, et al. 2019. Dynamical phase transitions and cation orientation–dependent photoconductivity in $CH(NH_2)_2PbBr_3$. *ACS Mater. Lett.* 1:260–64
77. Mozur EM, Maughan AE, Cheng Y, Huq A, Jalarvo N, et al. 2017. Orientational glass formation in substituted hybrid perovskites. *Chem. Mater.* 29:10168–77
78. Mozur EM, Hope MA, Trowbridge JC, Halat DM, Daemen LL, et al. 2020. Cesium substitution disrupts concerted cation dynamics in formamidinium hybrid perovskites. *Chem. Mater.* 32:6266–77
79. Selig O, Sadhanala A, Müller C, Lovrincic R, Chen Z, et al. 2017. Organic cation rotation and immobilisation in pure and mixed methylammonium lead-halide perovskites. *J. Am. Chem. Soc.* 139:4068–74
80. Li J, Bouchard M, Reiss P, Aldakov D, Pouget S, et al. 2018. Activation energy of organic cation rotation in $CH_3NH_3PbI_3$ and $CD_3NH_3PbI_3$: quasi-elastic neutron scattering measurements and first-principles analysis including nuclear quantum effects. *J. Phys. Chem. Lett.* 9:3969–77
81. Kanno S, Imamura Y, Saeki A, Hada M. 2017. Rotational energy barriers and relaxation times of the organic cation in cubic methylammonium lead/tin halide perovskites from first principles. *J. Phys. Chem. C* 121:14051–59
82. Xu Q, Eguchi T, Nakayama H, Nakamura N, Kishita M. 1991. Molecular motions and phase transitions in solid $CH_3NH_3PbX_3$ (X = Cl, Br, I) as studied by NMR and NQR. *Z. Naturforsch. A* 46:240–46
83. Furukawa Y, Nakamura D. 1989. Cationic dynamics in the crystalline phases of $(CH_3NH_3)PbX_3$ (X: Cl, Br) as studied by proton magnetic resonance techniques. *Z. Naturforsch. A* 44:1122–26
84. Knop O, Wasylishen RE, White MA, Cameron TS, Van Oort MJM. 1990. Alkylammonium lead halides. Part 2. $CH_3NH_3PbX_3$ (X = Cl, Br, I) perovskites: cuboctahedral halide cages with isotropic cation reorientation. *Can. J. Chem.* 68:412–22
85. Li B, Long R, Xia Y, Mi Q. 2018. All-inorganic perovskite $CsSnBr_3$ as a thermally stable, free-carrier semiconductor. *Angew. Chem. Int. Ed.* 57:13154–58
86. Marronnier A, Roma G, Carignano MA, Bonnassieux Y, Katan C, et al. 2019. Influence of disorder and anharmonic fluctuations on the dynamical Rashba effect in purely inorganic lead-halide perovskites. *J. Phys. Chem. C* 123:291–98
87. Kepenekian M, Robles R, Katan C, Sapori D, Pedesseau L, Even J. 2015. Rashba and Dresselhaus effects in hybrid organic–inorganic perovskites: from basics to devices. *ACS Nano* 9:11557–67
88. Mosconi E, Etienne T, De Angelis F. 2017. Rashba band splitting in organohalide lead perovskites: bulk and surface effects. *J. Phys. Chem. Lett.* 8:2247–52
89. Wang J, Zhang C, Liu H, McLaughlin R, Zhai Y, et al. 2019. Spin-optoelectronic devices based on hybrid organic–inorganic trihalide perovskites. *Nat. Commun.* 10:129
90. Glinka YD, Cai R, Li J, Lin X, Xu B, et al. 2019. Distinguishing between dynamical and static Rashba effects in hybrid perovskite nanocrystals using transient absorption spectroscopy. arXiv:1909.03605 [physics]
91. Wu B, Yuan H, Xu Q, Steele JA, Giovanni D, et al. 2019. Indirect tail states formation by thermal-induced polar fluctuations in halide perovskites. *Nat. Commun.* 10:484

92. Niesner D, Hauck M, Shrestha S, Levchuk I, Matt GJ, et al. 2018. Structural fluctuations cause spin-split states in tetragonal (CH_3NH_3)PbI_3 as evidenced by the circular photogalvanic effect. *PNAS* 115:9509–14
93. Etienne T, Mosconi E, De Angelis F. 2016. Dynamical origin of the Rashba effect in organohalide lead perovskites: a key to suppressed carrier recombination in perovskite solar cells? *J. Phys. Chem. Lett.* 7:1638–45
94. Motta C, El Mellouhi F, Kais S, Tabet N, Alharbi F, Sanvito S. 2015. Revealing the role of organic cations in hybrid halide perovskite $CH_3NH_3PbI_3$. *Nat. Commun.* 6:7026
95. Ryu H, Park DY, McCall K, Byun HR, Lee Y, et al. 2020. Static Rashba effect by surface reconstruction and photon recycling of the dynamic Rashba gap in halide perovskite single crystals. *J. Am. Chem. Soc.* 142:21059–67
96. Frost JM, Walsh A. 2016. What is moving in hybrid halide perovskite solar cells? *Acc. Chem. Res.* 49:528–35
97. Shikoh AS, Polyakov AY, Smirnov NB, Shchemerov IV, Saranin DS, et al. 2020. Ion dynamics in single and multi-cation perovskite. *ECS J. Solid State Sci. Technol.* 9:065015
98. Slotcavage DJ, Karunadasa HI, McGehee MD. 2016. Light-induced phase segregation in halide-perovskite absorbers. *ACS Energy Lett.* 1:1199–205
99. Rakita Y, Lubomirsky I, Cahen D. 2019. When defects become 'dynamic.' Halide perovskites: a new window on materials? *Mater. Horiz.* 6:1297–305
100. Chen Y, Tan S, Li N, Huang B, Niu X, et al. 2020. Self-elimination of intrinsic defects improves the low-temperature performance of perovskite photovoltaics. *Joule* 4:1961–76
101. Christians JA, Schulz P, Tinkham JS, Schloemer TH, Harvey SP, et al. 2018. Tailored interfaces of unencapsulated perovskite solar cells for >1,000 hour operational stability. *Nat. Energy* 3:68–74
102. Svane KL, Forse AC, Grey CP, Kieslich G, Cheetham AK, et al. 2017. How strong is the hydrogen bond in hybrid perovskites? *J. Phys. Chem. Lett.* 8:6154–59
103. Dastidar S, Egger DA, Tan LZ, Cromer SB, Dillon AD, et al. 2016. High chloride doping levels stabilize the perovskite phase of cesium lead iodide. *Nano Lett.* 16:3563–70
104. Chen T, Foley BJ, Park C, Brown CM, Harriger LW, et al. 2016. Entropy-driven structural transition and kinetic trapping in formamidinium lead iodide perovskite. *Sci. Adv.* 2:e1601650
105. Poglitsch A, Weber D. 1987. Dynamic disorder in methylammoniumtrihalogenoplumbates (II) observed by millimeter-wave spectroscopy. *J. Chem. Phys.* 87:6373–78
106. Laurita G, Fabini DH, Stoumpos CC, Kanatzidis MG, Seshadri R. 2017. Chemical tuning of dynamic cation off-centering in the cubic phases of hybrid tin and lead halide perovskites. *Chem. Sci.* 8:5628–35
107. Songvilay M, Wang Z, Sakai VG, Guidi T, Bari M, et al. 2019. Decoupled molecular and inorganic framework dynamics in $CH_3NH_3PbCl_3$. *Phys. Rev. Mater.* 3:125406
108. Brivio F, Frost JM, Skelton JM, Jackson AJ, Weber OJ, et al. 2015. Lattice dynamics and vibrational spectra of the orthorhombic, tetragonal, and cubic phases of methylammonium lead iodide. *Phys. Rev. B* 92:144308
109. Leguy AMA, Goñi AR, Frost JM, Skelton J, Brivio F, et al. 2016. Dynamic disorder, phonon lifetimes, and the assignment of modes to the vibrational spectra of methylammonium lead halide perovskites. *Phys. Chem. Chem. Phys.* 18:27051–66
110. Maughan AE, Ganose AM, Candia AM, Granger JT, Scanlon DO, Neilson JR. 2018. Anharmonicity and octahedral tilting in hybrid vacancy-ordered double perovskites. *Chem. Mater.* 30:472–83
111. Whalley LD, Frost JM, Jung YK, Walsh A. 2017. Perspective: theory and simulation of hybrid halide perovskites. *J. Chem. Phys.* 146:220901
112. Govinda S, Kore BP, Bokdam M, Mahale P, Kumar A, et al. 2017. Behavior of methylammonium dipoles in MAPbX_3 (X = Br and I). *J. Phys. Chem. Lett.* 8:4113–21
113. Govinda S, Kore BP, Swain D, Hossain A, De C, et al. 2018. Critical comparison of FAPbX_3 and MAPbX_3 (X = Br and Cl): How do they differ? *J. Phys. Chem. C* 122:13758–66
114. Hutter EM, Gélvez-Rueda MC, Osherov A, Bulović V, Grozema FC, et al. 2017. Direct–indirect character of the bandgap in methylammonium lead iodide perovskite. *Nat. Mater.* 16:115–20

115. Miyata A, Mitioglu A, Plochocka P, Portugall O, Wang JTW, et al. 2015. Direct measurement of the exciton binding energy and effective masses for charge carriers in organic–inorganic tri-halide perovskites. *Nat. Phys.* 11:582–87
116. Fabini DH, Stoumpos CC, Laurita G, Kaltzoglou A, Kontos AG, et al. 2016. Reentrant structural and optical properties and large positive thermal expansion in perovskite formamidinium lead iodide. *Angew. Chem. Int. Ed.* 55:15392–96
117. Keshavarz M, Ottesen M, Wiedmann S, Wharmby M, Küchler R, et al. 2019. Tracking structural phase transitions in lead-halide perovskites by means of thermal expansion. *Adv. Mater.* 31:1900521
118. Schueller EC, Laurita G, Fabini DH, Stoumpos CC, Kanatzidis MG, Seshadri R. 2018. Crystal structure evolution and notable thermal expansion in hybrid perovskites formamidinium tin iodide and formamidinium lead bromide. *Inorg. Chem.* 57:695–701
119. Carignano MA, Saeed Y, Aravindh SA, Roqan IS, Even J, Katan C. 2016. A close examination of the structure and dynamics of $HC(NH_2)_2PbI_3$ by MD simulations and group theory. *Phys. Chem. Chem. Phys.* 18:27109–18
120. Chen T, Chen WL, Foley BJ, Lee J, Ruff JPC, et al. 2017. Origin of long lifetime of band-edge charge carriers in organic–inorganic lead iodide perovskites. *PNAS* 114:7519–24
121. Grannan ER, Randeria M, Sethna JP. 1990. Low-temperature properties of a model glass. I. Elastic dipole model. *Phys. Rev. B* 41:7784–99
122. Kubicki D, Prochowicz D, Hofstetter A, Pechy P, Zakeeruddin SM, et al. 2017. Cation dynamics in mixed-cation $(MA)_x(FA)_{1-x}PbI_3$ hybrid perovskites from solid-state NMR. *J. Am. Chem. Soc.* 139:10055–61
123. Kanno S, Imamura Y, Hada M. 2017. Theoretical study on rotational controllability of organic cations in organic–inorganic hybrid perovskites: hydrogen bonds and halogen substitution. *J. Phys. Chem. C* 121:26188–95
124. Yang W, Igbari F, Lou Y, Wang Z, Liao L. 2020. Tin halide perovskites: progress and challenges. *Adv. Energy Mater.* 10:1902584
125. Ganose AM, Savory CN, Scanlon DO. 2017. Beyond methylammonium lead iodide: prospects for the emergent field of ns^2 containing solar absorbers. *Chem. Commun.* 53:20–44
126. Stoumpos CC, Frazer L, Clark DJ, Kim YS, Rhim SH, et al. 2015. Hybrid germanium iodide perovskite semiconductors: active lone pairs, structural distortions, direct and indirect energy gaps, and strong nonlinear optical properties. *J. Am. Chem. Soc.* 137:6804–19
127. Yamada K, Kuranaga Y, Ueda K, Goto S, Okuda T, Furukawa Y. 1998. Phase transition and electric conductivity of $ASnCl_3$ (A = Cs and CH_3NH_3). *Bull. Chem. Soc. Jpn.* 71:127–34
128. Yamada K, Mikawa K, Okuda T, Knight KS. 2002. Static and dynamic structures of $CD_3ND_3GeCl_3$ studied by TOF high resolution neutron powder diffraction and solid state NMR. *J. Chem. Soc. Dalton Trans.* 2002:2112–18
129. Herz LM. 2018. How lattice dynamics moderate the electronic properties of metal-halide perovskites. *J. Phys. Chem. Lett.* 9:6853–63
130. Guedes-Sobrinho D, Guilhon I, Marques M, Teles LK. 2019. Thermodynamic stability and structural insights for $CH_3NH_3Pb_{1-x}Si_xI_3$, $CH_3NH_3Pb_{1-x}Ge_xI_3$, and $CH_3NH_3Pb_{1-x}Sn_xI_3$ hybrid perovskite alloys: a statistical approach from first principles calculations. *Sci. Rep.* 9:11061
131. Swainson I, Chi L, Her JH, Cranswick L, Stephens P, et al. 2010. Orientational ordering, tilting and lone-pair activity in the perovskite methylammonium tin bromide, $CH_3NH_3SnBr_3$. *Acta Crystallogr. B* 66:422–29
132. Rosales BA, Wei L, Vela J. 2019. Synthesis and mixing of complex halide perovskites by solvent-free solid-state methods. *J. Solid State Chem.* 271:206–15
133. Liu F, Wang F, Hansen KR, Zhu XY. 2019. Bimodal bandgaps in mixed cesium methylammonium lead bromide perovskite single crystals. *J. Phys. Chem. C* 123:14865–70
134. Askar AM, Bernard GM, Wiltshire B, Shankar K, Michaelis VK. 2017. Multinuclear magnetic resonance tracking of hydro, thermal, and hydrothermal decomposition of $CH_3NH_3PbI_3$. *J. Phys. Chem. C* 121:1013–24
135. Senocrate A, Kim GY, Grätzel M, Maier J. 2019. Thermochemical stability of hybrid halide perovskites. *ACS Energy Lett.* 4:2859–70

136. Aziz A, Aristidou N, Bu X, Westbrook RJE, Haque SA, Islam MS. 2020. Understanding the enhanced stability of bromide substitution in lead iodide perovskites. *Chem. Mater.* 32:400–9
137. Cordero F, Craciun F, Trequattrini F, Generosi A, Paci B, et al. 2019. Stability of cubic $FAPbI_3$ from X-ray diffraction, anelastic, and dielectric measurements. *J. Phys. Chem. Lett.* 10:2463–69
138. Schelhas LT, Li Z, Christians JA, Goyal A, Kairys P, et al. 2019. Insights into operational stability and processing of halide perovskite active layers. *Energy Environ. Sci.* 12:1341–48
139. Poorkazem K, Kelly TL. 2018. Compositional engineering to improve the stability of lead halide perovskites: a comparative study of cationic and anionic dopants. *ACS Appl. Energy Mater.* 1:181–90
140. Chen L, Tan YY, Chen ZX, Wang T, Hu S, et al. 2019. Toward long-term stability: single-crystal alloys of cesium-containing mixed cation and mixed halide perovskite. *J. Am. Chem. Soc.* 141:1665–71
141. Leppert L, Reyes-Lillo SE, Neaton JB. 2016. Electric field– and strain-induced Rashba effect in hybrid halide perovskites. *J. Phys. Chem. Lett.* 7:3683–89
142. Rodova M, Brozek J, Knizek K, Nitsch K. 2003. Phase transitions in ternary caesium lead bromide. *J. Therm. Anal. Calorim.* 71:667–73
143. Young J, Rondinelli JM. 2016. Octahedral rotation preferences in perovskite iodides and bromides. *J. Phys. Chem. Lett.* 7:918–22
144. Lee JH, Bristowe NC, Bristowe PD, Cheetham AK. 2015. Role of hydrogen-bonding and its interplay with octahedral tilting in $CH_3NH_3PbI_3$. *Chem. Commun.* 51:6434–37
145. Franz A, Többens DM, Schorr S. 2016. Interaction between cation orientation, octahedra tilting and hydrogen bonding in methylammonium lead triiodide. *Cryst. Res. Technol.* 51:534–40
146. Yin T, Fang Y, Fan X, Zhang B, Kuo JL, et al. 2017. Hydrogen-bonding evolution during the polymorphic transformations in $CH_3NH_3PbBr_3$: experiment and theory. *Chem. Mater.* 29:5974–81
147. Li N, Luo Y, Chen Z, Niu X, Zhang X, et al. 2020. Microscopic degradation in formamidinium-cesium lead iodide perovskite solar cells under operational stressors. *Joule* 4:1743–58
148. Correa-Baena JP, Luo Y, Brenner TM, Snaider J, Sun S, et al. 2019. Homogenized halides and alkali cation segregation in alloyed organic-inorganic perovskites. *Science* 363:627–31
149. Hutter EM, Muscarella LA, Wittmann F, Versluis J, McGovern L, et al. 2020. Thermodynamic stabilization of mixed-halide perovskites against phase segregation. *Cell Rep. Phys. Sci.* 1:100120
150. Lee MM, Teuscher J, Miyasaka T, Murakami TN, Snaith HJ. 2012. Efficient hybrid solar cells based on meso-superstructured organometal halide perovskites. *Science* 338:643–47
151. López CA, Álvarez-Galván MC, Martínez-Huerta MV, Fernández-Díaz MT, Alonso JA. 2019. Dynamic disorder restriction of methylammonium (MA) groups in chloride-doped $MAPbBr_3$ hybrid perovskites: a neutron powder diffraction study. *Chem. Eur. J.* 25:4496–500